Artificial Intelligence in Agriculture 5 (2021) 233–239

Contents lists available at ScienceDirect

Artificial Intelligence in Agriculture

journal homepage: http://www.keaipublishing.com/en/journals/artificial-intelligence-in-agriculture/

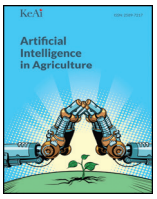

Freeform path fitting for the minimisation of the number of transitions between headland path and interior lanes within agricultural fields

Mogens Graf Plessen *

MGP is an independent researcher

ARTICLE INFO

Article history:
Received 6 March 2021
Received in revised form 10 October 2021
Accepted 10 October 2021
Available online 26 October 2021

Keywords:
In-field path planning
Freeform path fitting
Agricultural logistics

ABSTRACT

Within the context of in-field path planning this paper discusses freeform path fitting for the minimisation of the number of transitions between headland path and interior lanes within agricultural fields. This topic is motivated by two observations. Due to crossings of tyre traces such transitions in practice often cause an increase of compacted area. Furthermore, for very tight angles between headland path and interior lanes undesired hairpin turns may become necessary due to the limited agility of in-field operating tractors. By minimising the number of interior lanes both detrimental effects can be mitigated. The potential of minimising the number of interior lanes by freeform path fitting is evaluated on 10 non-convex real-world fields including obstacle areas, and compared to the more common technique of fitting straight interior lanes.

1. Introduction

According to Ahumada and Villalobos (2009) there are four main functional sectors for the agri-food supply chain: production, harvesting, storage and distribution. Optimising logistics and routing play an important role in all of the four functional areas for improved supply chain efficiency. Furthermore, according to Sorensen and Bochtis (2010) it can be distinguished between in-field, inter-field, inter-sector and inter-regional logistics. This paper relates to the first functional area of the agri-food supply chain, i.e., production, and further to in-field logistics. The difficulty of in-field logistics arises from the vast variety of field shapes encountered in practice. In this perspective Oksanen (2013) presented eight indices for measuring the complexity of field shapes. For an application, see Janulevicius et al. (2019) who studied the effect of different field width-to-length ratios on tractor performance measures such as fuel consumption and exhaust emissions when ploughing.

For in-field logistics it can be differentiated between three hierarchical planning layers: (i) the fitting of lanes within field contours, (ii) route planning for the traversal of these lanes, and (iii) trajectory planning accounting for agility and actuation constraints of the in-field operating vehicle to smooth out final paths. This paper focuses on the first hierachical layer and, in particular, how freeform path fitting compares to the more common method of fitting straights as interior lanes. For background, the coverage of agricultural fields growing, e.g., cereals or rapeseed requires lanes to be fitted within field contours such that in-field operating machinery can repeatedly travel along them during the work cycle after seeding and before harvest. These traversals typically occur many times throughout the year for multiple spraying and fertilizing applications.

Oksanen and Visala (2009) presented two greedy algorithms for field coverage path planning. The first algorithm splits a single field using a trapezoidal split-and-merge scheme into multiple smaller convex or near convex subfields that are then simpler to drive or operate using the best driving direction and best selection of subfields. Straight driving lanes are assumed. In contrast, in the second algorithm the path is planned on the basis of the machine's current state and the search over a limited search horizon is on the next lanes instead of the next subfield. Lanes are now permitted to be curved. Note that for both algorithms multiple different path patterns may result within the same field. Thus, in general, also multiple new headland paths must be generated within the field in order to bound the different pattern regions, whereby segments of headland paths coincide for neighbouring regions. Consequently, more transitions between interior lanes and headlands and more compacted areas result. Thus, while partitioning of a field into multiple subfields may be inevitable for strongly non-convex field shapes that demand very different driving behaviour, it also comes at a cost.

Hameed et al. (1086) computed optimal driving directions for straight interior lanes based on the minimization of overlapped area using a genetic algorithm, before optimal routing is determined based on the minimization of the non-working distance. Freeform path planning is not discussed. Results are evaluated on two obstacle-free test fields.

* Corresponding author.
E-mail address: mgplessen@gmail.com (M. Graf Plessen).

https://doi.org/10.1016/j.aiia.2021.10.004

Nomenclature

Symbols

d	Interpolation distance (m)
ε	Hyperparameter for interpolation (%)
N_l	Number of interior lanes (-)
ΔN_l	Difference in number of interior lanes (-) or (%)
θ	Angle coordinate (°)
$\Delta\theta_{\max}$	Maximum permissible angle difference (°)
w	Operating width (inter-lane distance) (m)
(x, y)	Position coordinates (m)

Abbreviation

UTM	Universal Transverse Mercator coordinate system

Hameed et al. (2010) presented a method for automated generation of guidance lines for operational field planning. A geometrical representation of the field is constructed as a geometrical entity comprising discrete geometric primitives such as points, lines, and polygons. For their generation of parallel lanes the concept of "longest edge" of the field or partitioned subfields is crucial. It is selected to determine the driving direction. The curved edge is determined as a collection of sequential straight edges satisfying the criterion that the angle between two successive edges is less than or equal to a threshold. Complex field shapes are partitioned into a number of simpler subfields, typically convex polygons.

Jin and Tang (2011) accounted for 3D terrain topography. Four critical tasks were therefore addressed: terrain modeling and representation, coverage cost analysis, terrain decomposition, and determining a suitable reference path such that by offsetting a lane pattern for full field coverage is obtained. Field boundary segments and topographic terrain contour lines were considered as the two categories for reference curve candidates. In Guo (2018) a similar study is discussed, where soil and water conservation is also considered for the design of reference curves. In Spekken et al. (2016) 3D terrain topograpgy is also examined. The objective was soil loss minimisation for sugarcane production. Therefore, "hybrid" curves were proposed as reference paths. These are generated by continuously offsetting multiple field contour segments towards each other until the hybrid curve is formed as their intersection points. While corresponding results were found to be beneficial, a disadvantage of this method is that the shape of the hybrid curve does not follow any particular segment of the field contour such that realisation in practice is difficult due to lack of nature-given visual reference landmarks.

Once lanes are fitted within field contours available methods from the literature can be employed for the two other aforementioned hierarchical planning layers (routing algorithms for traversal of lanes and trajectory planning for final path smoothing) including, for example, Jensen et al., 2015, Bochtis et al., 2013, Hameed et al., 2016, Yu et al., 2015, Spekken et al., 2015, Seyyedhasani and Dvorak, 2018, Plessen, 2018, Paraforos et al., 2018 and Backman et al., 2012. Consider also Plessen, 2019 for the coupling of crop assignment and and vehicle routing.

To summarise, given UTM-coordinates of a field contour and of all its in-field obstacles, the first step is to fit interior lanes. Because of being the primary step lane fitting presents the foundation for all upstream logistical optimisation layers on top, including routing, trajectory planning and even multi-robot coordination. This underlines the importance of lane fitting. Furthermore, as satellite pictures show, the vast majority of fields in practice is fitted with straight lanes. Obviously, straights are attractive due to their simplicity and absence of turning. On the other hand, almost all fields are irregularly and very often even (strongly) non-convexly shaped. In view of this discrepancy the research question arises whether freeform path fitting may yet be underestimated for improved agricultural in-field operations and merit more studying. This argument is supported particularly by the fact that straights can be considered as just a subset of the more general class of freeform paths. It is therefore expected that freeform paths can produce improved or at least equally good solutions for a variety of optimisation objectives.

Within this context the motivation and contribution of this paper is to discuss the potential of freeform path fitting for the minimisation of the number of transitions between headland path and interior lanes within agricultural fields. As a proxy therefore, the number of interior lanes is minimised. This is achieved by optimised freeform fitting of interior lanes to arbitrarily non-convexly shaped field areas, that also may include obstacle areas. While freeform fitting of interior lanes is not new and sometimes in practice even performed intuitively by farmers, e.g., on wavy or curvedly shaped fields, the outcome of a quantitative comparison with respect to optimal straights fitting and explicit evaluation of the number of interior lanes that can be saved in real-world scenarios is not obvious.

The remaining paper is organised as follows: problem modeling and proposed solution, numerical results and the conclusion are described in Sections 2–4.

2. Problem modeling and proposed solution

Figs. 1 and 2 introduce basic terminology. See Figs. 3 and 4 for real-world visualisation on satellite images and problem motivation.

Problem input are location data of the *field contour* and all available *obstacle contours*. In a first step, the field contour is eroded to generate the *headland path*. Similarly, obstacle contours are dilated to construct *obstacle headland paths*. In a second step, a *reference path* is selected as a partial segment of the headland path. In a third step, this reference is offset to generate a grid of *interior lanes* fitted within field contours with inter-lane distance selected as the machinery operating width w. In this paper it is iterated over the selection of the reference path according to the criterion of minimising the total number of interior lanes denoted by N_l.

A candidate location point, $(x_k^{(i+1)}, y_k^{(i+1)})$, in the next interior lane $i+1$ is generated based on two points, $(x_k^{(i)}, y_k^{(i)})$ and $(x_{k+1}^{(i)}, y_{k+1}^{(i)})$, in the previous interior lane i, according to

$$\theta_k^{(i)} = \arctan\left(\frac{y_{k+1}^{(i)} - y_k^{(i)}}{x_{k+1}^{(i)} - x_k^{(i)}}\right), \tag{1a}$$

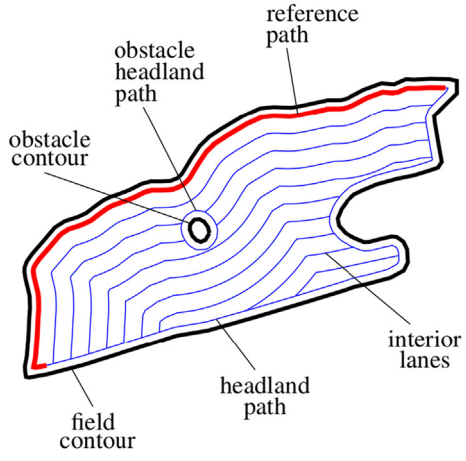

Fig. 1. Illustration of notation. Obstacles may represent tree islands, ponds, power pole masts, and so forth. The optimisation objective is to select the reference path (red) optimally as a partial segment of the headland path such as to minimise the total number of interior lanes subject to constraints.

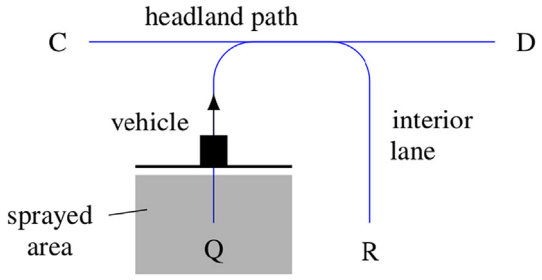

Fig. 2. Abstract visualisation with the definitions of *headland path* and *interior lanes* along which a vehicle (e.g., with spraying implement) might travel from location Q towards R or D.

$$\begin{bmatrix} x_k^{(i+1)} \\ y_k^{(i+1)} \end{bmatrix} = \begin{bmatrix} \frac{x_k^{(i)} + x_{k+1}^{(i)}}{2} \\ \frac{y_k^{(i)} + y_{k+1}^{(i)}}{2} \end{bmatrix} + w \begin{bmatrix} \cos(\theta_k^{(i)} + \frac{\pi}{2}) \\ \sin(\theta_k^{(i)} + \frac{\pi}{2}) \end{bmatrix}, \tag{1b}$$

before it is tested for pruning and constraints. Similarly the headland path and all obstacle headland paths are constructed, whereby the offsetting distance is here $w/2$, i.e., half the operating width.

An implementation detail is discussed. After fitting of any interior lane its location data points are spatially extended by interpolation such that the distance between any 2 consecutive locations describing the interior lane is at most of length $d > 0$. This is relevant for pruning and permits to work with *circle inclusion checks* to determine if a candidate location $(x_k^{(i+1)}, y_k^{(i+1)})$ according to Eq. (1b) maintains a distance of w to all lane segments describing the previous interior lane i. Obviously this holds by definition for the lane segment described by $(x_k^{(i)}, y_k^{(i)})$ and $(x_{k+1}^{(i)}, y_{k+1}^{(i)})$. However, it may in general not hold for all lane segments and therefore may require pruning. The preferred method for the selection of $d > 0$ is discussed next. See also Fig. 5 for visualisation. The fundamental idea is to work with circle inclusion checks to determine if a candidate location point P maintains with desired ε-confidence (e.g., $\varepsilon = 99\%$) distance $w>0$ from any piecewise lane segment that concatenatedly describe the previous interior lane. With respect to Fig. 5, the constraint $h > \varepsilon w$ can therefore be formulated. Using elementary geometric arguments this translates to a desired interpolation distance of

$$d < 2w\sqrt{1-\varepsilon^2}. \tag{2}$$

In contrast, for the headland and obstacle headland paths it is $d < 2\frac{w}{2}\sqrt{1-\varepsilon^2}$ because of their target-distance of half the operating width with respect to the field and obstacle contours, respectively. In final evaluation experiments it is set $w = 36$m and $\varepsilon = 99\%$, which implies a spatial interpolation grid of at least 5 m along headland and obstacle headland paths and 10m along interior lanes. Note that when collecting field and obstacle contour data points from real-world fields, these typically are already recorded to be sufficiently well shape-defining. Therefore, interpolation points along the field and obstacle contours are here added spatially only for improved constraint checking. The field and obstacle shape as defined by originally recorded contour data is not altered.

A pruned point does not abort interior lanes construction. It merely filters out some location points. In contrast, any constraint violation results in the dismissal of the entire corresponding reference path candidate. Before discussing constraints in detail, two more implementation details are therefore described. First, the last point of any interior lane is linearly extrapolated (leveraging the penultimate point for the direction) to obtain the intersection with the headland path. Second, after fitting of any interior lane its coordinates are extended by above discussed spatial interpolation technique with spacing according to Eq. (2).

Constraints are discussed. First, any crossings of any two interior lanes are prohibited. Second, too tight turns (expressed as the change of directions between two adjacent lane segments) are not admitted such that candidates with

$$|\theta_{k+1}^{(i)} - \theta_k^{(i)}| > \Delta\theta_{\max}, \tag{3}$$

for any $k = 1, \ldots, |\{\theta_k^{(i)}\}|-1, \ \forall i = 1, \ldots, N_l$ are dismissed. In experiments the threshold was set to $\Delta\theta_{\max} = 135°$. This somewhat aggressive choice is here motivated to determine a conservative upper bound on the saving potential of freeform path fitting. Third, also interpretable as a tight angle constraint to maintain a minimum w-distance among coordinates of each lane itself it is set

Fig. 3. Visualisation of real-world transitions between headland path and interior lanes. As illustrated, the transitions between headland path and interior lanes can be "messy" in the sense that these often cause an increased amount of compacted field areas due to crossings of tyre traces. This motivates the minimisation of such transitions, and therefore to minimise the number of interior lanes as a proxy.

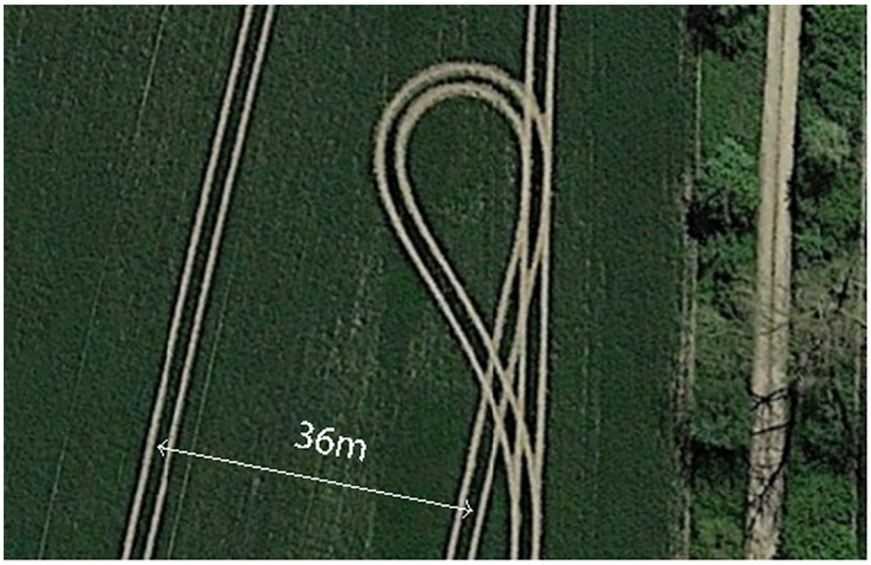

Fig. 4. For very tight angles between headland path and interior lanes undesired hairpin turns may become necessary due to the limited agility of in-field operating tractors. The more transitions between headland path and interior lanes the higher also the probability that such turns may occur, in particular, for complex fields. This provides the second motivation for the minimisation of the number of interior lanes by freeform path fitting.

$$\sqrt{(x_j^{(i)}-x_k^{(i)})^2+(y_j^{(i)}-y_k^{(i)})^2} > w, \tag{4}$$

for all $k=1,\dots,|\{x_k^{(i)}\}|$, $\forall j=k+\Delta k,\dots,|\{x_k^{(i)}\}|$, $\forall i=1,\dots,N_l$, and with hyperparameter $\Delta k>0$ denoting a blocking index interval. In experiments it was set $\Delta k=20$.

The operating width w is given by available machinery hardware setup. For example, for spraying applications on fields growing cereals or rapeseed in central Europe it is often $w=36$m or $w=24$m. To sum up, for the proposed method three hyperparameters occur: $\varepsilon\in[0,1]$, $\Delta\theta_{\max}\in[0,\pi]$ and $\Delta k>0$. For the latter a lower bound can be determined as $\Delta k>\frac{w}{d}$. Then all three hyperparameters are lower bounded. The choice of $\varepsilon=99\%$ as discussed above is reasonable for an accurate interpolation grid. To account for two operating widths one may heuristically select $\Delta k\propto\lceil\frac{2w}{d}\rceil$. Then, only one shaping hyperparameter, $\Delta\theta_{\max}\in[0,\pi]$, remains.

As a proxy for the task of minimising the number of transitions between headland path and interior lanes the minimisation of the number of interior lanes, N_l, is selected as the optimisation criterion. This is valid since for every field run every interior lane must typically be covered exactly *once*, thus requiring exactly one entrance and one exit transition from and to the headland path, respectively.

Before discussing data-dependent results for 10 real-world fields, the comparative method of fitting *straights* as interior lanes is reconsidered.

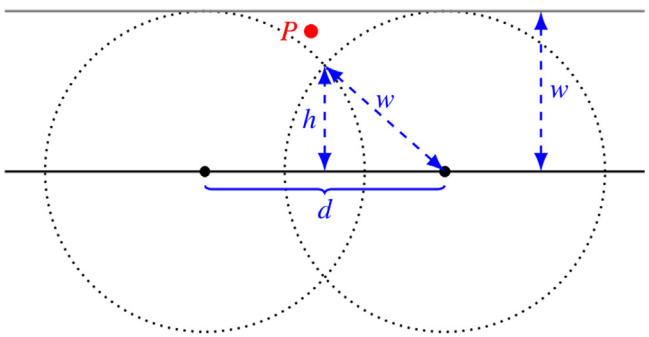

Fig. 5. Derivation of spatial interpolation distance $d>0$.

Remark 1. The method of fitting straights as interior lanes can, in general, be regarded as a special case of freeform path fitting. Instead of selecting a reference path defined by a segment or *multiple* sequential location data points along the headland path for the latter scenario, it is defined by only *two* points for the former case for the generation of straight interior lanes. For rectangular field shapes this method is optimal. However, for the general case of arbitrarily shaped fields optimality of straight interior lanes is not guaranteed. Since the problem class of straights fitting is included as a subset in the problem class of freeform path fitting, the latter will always be at least as good as the former for any objective, including, e.g., minimisation of total accumulated path length of interior lanes or total travel time along interior lanes. The critical disadvantage of freeform path fitting is the requirement of at least one shaping hyperparameter to constrain desired turning or curvatures of resulting paths. In contrast, for straights fitting no such shaping hyperparameter is required. Instead, it must solely be accounted for the physical machine operating width.

3. Numerical results and discussion

The potential of minimising the number of interior lanes by freeform path fitting is evaluated on a variety of 10 real-world fields, and compared to the more common technique of fitting straight interior lanes. For the latter solution, the orientation of straights is also optimised to minimise the number of interior lanes N_l.

Table 1
Data source: latitude and longitude locations of 10 real-world fields.

Field	Latitude	Longitude
1	53.59770954380925	11.88127909152601
2	53.61823042559124	11.14953204162411
3	53.72742495969927	11.66364803235982
4	54.18747037363151	10.36452303204824
5	53.57461963247646	11.0042633468972
6	53.61806582717429	11.15610791641177
7	54.19332379320142	10.43562800256227
8	53.69782126551283	11.71264284008849
9	53.77552865867575	11.18667955767437
10	54.28618542958617	10.37204982106118

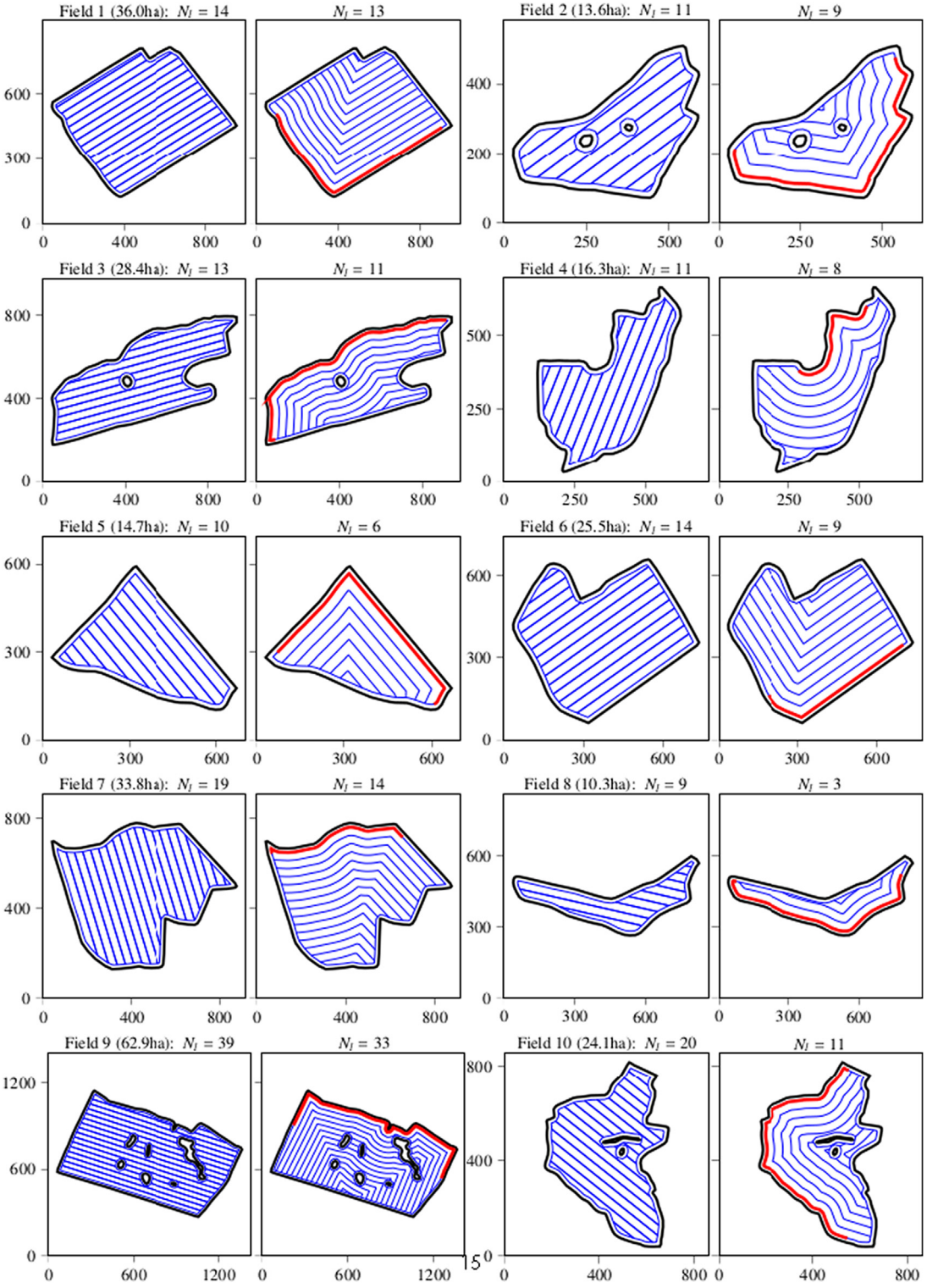

Fig. 6. Results for 10 real-world fields. The assumed operating width is $w = 36$m. Optimal solutions of fitting straights and freeform paths for the minimisation of N_l are displayed in the left and right subplot for each field, respectively. Axes are denominated in meters. Latitude and longitude of all 10 fields are summarized in Table 1.

Field data was obtained from satellite images in Google Earth (http://earth.google.com) by tracking field contours and contours of all in-field obstacle areas (such as e.g., tree islands), before exporting those raw location data points as .kml-files and feeding it to proposed algorithm. Fields were selected to emphasize effects of the compared path fitting methods on a variety of very differently shaped fields as well as with and without in-field obstacle areas. The latitude and longitude locations of all fields are summarized in Table 1, which permits to replicate field data. By contacting the author the ,kml-data files will also be available upon request.

Field sizes vary between 10.3 ha and 62.9 ha. Results are summarised in Fig. 6 and Table 2. The following observations are made.

First, savings range from −1 lane to -9 lanes. Percentage-wise, this implies the number of interior lanes could be reduced by −7% to

Table 2
Summary of quantitative results displayed in Fig. 6.

Field	Size (ha)	$N_l^{\text{straights}}$	N_l^{freeform}	ΔN_l	ΔN_l
1	36.0	14	13	−1	−7%
2	13.6	11	9	−2	−18%
3	28.4	13	11	−2	−15%
4	16.3	11	8	−3	−27%
5	14.7	10	6	−4	−40%
6	25.5	14	9	−5	−36%
7	33.8	19	14	−5	−26%
8	10.3	9	3	−6	−67%
9	62.9	39	33	−6	−15%
10	24.1	20	11	−9	−45%

−67% for freeform path fitting in comparison to optimal straights fitting. Note that for all fields a large operating width of $w = 36$ m is considered. For smaller operating widths savings scale linearly.

Second, while in some scenarios the optimised freeform path planning is intuitive such as for Field 8, it is surprising in other cases such as for Field 4. There are also subtle details about the exact optimal length of reference paths. In general, it therefore seems to be difficult to devise a reliable rule of thumb to select optimal reference paths. Thus, for general field shapes it clearly is best to turn to a data-dependent numerical optimisation method such as the proposed algorithm.

Third, the comparative method of fitting straights as interior lanes is discussed in more detail. For implementation simplicity it is in general desired to align straights to an approximately straight and typically also the longest segment of the field contour. For Field 1, Fig. 7 illustrates the resulting number of interior lanes N_l as a function of the rotation angle of interior lanes, whereby 0° implies a vertical or y-axis aligned interior lane. The minimising solution is obtained for $N_l = 14$ and is displayed in Fig. 6. When straight interior lanes were rotated by an additional 90° to obtain alignment with the field contour in the north east, $N_l = 17$ resulted. Then, savings for freeform path fitting would amount to −4 lanes and −24%. This underlines the importance of careful selection of the orientation for straight interior lanes. To stress this more, when performing the grid search for Field 3 a range of $N_l \in [13, 33]$ resulted, i.e., with possible variation of ±20 interior lanes. Finally, a detail with respect to Fig. 7 is discussed. The lack of exact symmetry, for example, visible for rotation angles 40–120° and 220–300°, is explained by the fact that the first interior lane is offset by distance w from the headland path in the rotated coordinate system. Consequently, a residual distance results at the last othogonal interior lane with respect to the headland path. Since the field shape is not perfectly symmetric for Field 1, the resulting function in Fig. 7 is also not exactly repeating with a phase-shift of 180°.

Fourth, as already pointed out in Remark 1, the strength of freeform path fitting is its flexibility in that it may (i) be used as a technique to also optimise *alternative* objectives besides the number of interior lanes or to optimise a weighted trade-off among different criteria, and (ii) that solutions can easily be constrained to limit the desired amount of steering and to tailor results to the vehicle's agility capabilities. In particular, for $\Delta\theta_{\max} = 0$ in Eq. (3) the solution of fitting straights as interior lanes, i.e., the *least-steering* solution, is recovered.

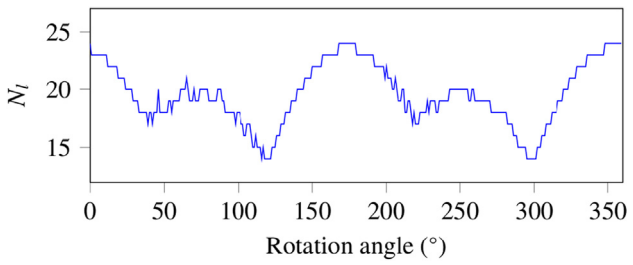

Fig. 7. Illustration of the effect of the rotation angle of straight interior lanes on the total number of interior lanes N_l for Field 1 in Fig. 6 and $w = 36$m. Note that N_l varies within a large range of 14 to 24 lanes.

Ultimately, after having fitted interior lanes within field contours one can on top (i) determine field coverage path plans, e.g., according to the methods in Plessen (2018) and Plessen (2019), before (ii) smoothing out trajectories by accounting for actuation constraints of the in-field operating vehicle, for example, according to the control methods in Backman et al. (2012) or Plessen and Bemporad (2017).

The most obvious disadvantage of freeform path fitting is the increased amount of steering that is needed along interior lanes. However, this is largely relevant only as long as there is a human vehicle driver. Currrently, such a driver would have to apply significantly increased effort for freeform path tracking. However, for an envisioned future with fully automated robotic field coverage this disadvantage is dismissed.

Because of path-fitting being the foundation for all upstream logistical optimization layers on top (including routing, trajectory planning and even multi-robot coordination) the subject of this research is crucial for the overall optimization of agricultural in-field work.

4. Conclusion

This paper contributed to the task of in-field path planning within agricultural fields by proposing a freeform path fitting method for the minimisation of the number of transitions between headland path and interior lanes. Therefore, as a proxy the minimisation of the number of interior lanes was selected as optimisation criterion. Spatial interpolation distances for pruning during the generation of interior lanes and constraints for the shaping of freeform paths were discussed. The potential of minimising the number of interior lanes by freeform path fitting was evaluated on 10 real-world fields and compared to the more common technique of fitting straight interior lanes. Field sizes varied between 10.3 ha and 62.9 ha with some including in-field obstacle areas. For an operating width of 36 m optimal straights fitting resulted in a range of between 9 to 39 interior lanes. In comparison, freeform path fitting resulted in savings in the range of −1 lane to −9 lanes or, perentage-wise speaking, in a reduction of the number of interior lanes by −7% to −67%.

This paper focused on the very clear to quantify number of interior lanes as the optimisation criterion, which served as a proxy for the minimisation of the number of transitions between headland path and interior lanes. For future work an alternative objective such as the total accumulated path length along interior lanes may be considered. Then, ideally three consecutive layers are evaluated for determining the optimal grid of interior lanes fitted within field contours. These three layers represent (i) selecting a reference path candidate as partial segment of the headland path and generating a corresponding grid of interior lanes as discussed in this paper, (ii) determining a routing solution for the coverage of all lane segments, before (iii) generating smoothed out trajectories accounting for agility and actuation constraints of the in-field operating vehicle, whereby the final detailed trajectory must also be planned such as to minimise spraying gaps. Similarly to as presented in this paper, it must then be iterated over reference path candidates before the total path length minimising solution is returned.

Declaration of Competing Interest

The author declare no conflict of interests.

References

Ahumada, O., Villalobos, J.R., 2009. Application of planning models in the agri-food supply chain: a review. Eur. J. Oper. Res. 196, 1–20.

Backman, J., Oksanen, T., Visala, A., 2012. Navigation system for agricultural machines: nonlinear model predictive path tracking. Comput. Electron. Agri. 82, 32–43.

Backman, J., Oksanen, T., Visala, A., 2012. Path generation method with steering rate constraint. ICPA (p. 15).
Bochtis, D.D., Srensen, C.G., Busato, P., Berruto, R., 2013. Benefits from optimal route planning based on b-patterns. Biosyst. Eng. 115, 389–395.
Guo, W., 2018. Application of geographic information system and automated guidance system in optimizing contour and terrace farming. Agriculture 8, 142.
Hameed, I., Bochtis, D., Srensen, C., Nremark, M., 2010. Automated generation of guidance lines for operational field planning. Biosyst. Eng. 107, 294–306.
Hameed, I.A., Bochtis, D., Sorensen, C., 2011. Driving angle and track sequence optimization for operational path planning using genetic algorithms. Appl. Eng. Agri. 27, 1077–1086.
Hameed, I.A., la Cour-Harbo, A., Osen, O.L., 2016. Side-to-side 3d coverage path planning approach for agricultural robots to minimize skip/overlap areas between swaths. Robot. Autonomous Syst. 76, 36–45.
Janulevicius, A., Sarauskis, E., Cipliene, A., Juostas, A., 2019. Estimation of farm tractor performance as a function of time efficiency during ploughing in fields of different sizes. Biosyst. Eng. 179, 80–93.
Jensen, M.F., Bochtis, D., Srensen, C.G., 2015. Coverage planning for capacitated field operations, part ii: Optimisation. Biosyst. Eng. 139, 149–164.
Jin, J., Tang, L., 2011. Coverage path planning on three-dimensional terrain for arable farming. J. Field Robot. 28, 424–440.
Oksanen, T., 2013. Shape-describing indices for agricultural field plots and their relationship to operational efficiency. Comput. Electron. Agri. 98, 252–259.
Oksanen, T., Visala, A., 2009. Coverage path planning algorithms for agricultural field machines. J. Field Robot. 26, 651–668.
Paraforos, D.S., Hbner, R., Griepentrog, H.W., 2018. Automatic determination of headland turning from auto-steering position data for minimising the infield non-working time. Comput. Electron. Agri. 152, 393–400.
Plessen, M.G., 2019. Coupling of crop assignment and vehicle routing for harvest planning in agriculture. Artif. Intell. Agri. 2, 99–109.
Plessen, M.G., 2019. Optimal in-field routing for full and partial field coverage with arbitrary non-convex fields and multiple obstacle areas. Biosyst. Eng. 186, 234–245.
Plessen, M.M.G., 2018. Partial field coverage based on two path planning patterns. Biosyst. Eng. 171, 16–29.
Plessen, M.M.G., Bemporad, A., 2017. Reference trajectory planning under constraints and path tracking using linear time-varying model predictive control for agricultural machines. Biosyst. Eng. 153, 28–41.
Seyyedhasani, H., Dvorak, J.S., 2018. Reducing field work time using fleet routing optimization. Biosyst. Eng. 169, 1–10.
Sorensen, C.G., Bochtis, D.D., 2010. Conceptual model of fleet management in agriculture. Biosyst. Eng. 105, 41–50.
Spekken, M., De Bruin, S., Molin, J.P., Sparovek, G., 2016. Planning machine paths and row crop patterns on steep surfaces to minimize soil erosion. Comput. Electron. Agri. 124, 194–210.
Spekken, M., Molin, J.P., Romanelli, T.L., 2015. Cost of boundary manoeuvres in sugarcane production. Biosyst. Eng. 129, 112–126.
Yu, X., Roppel, T.A., Hung, J.Y., 2015. An optimization approach for planning robotic field coverage. IECON Annual Conference of the IEEE Industrial Electronics Society. (pp. 004032–39)